ARMA 20–1519

An experimental investigation of the coupling between elastodynamic and hydraulic properties of naturally fractured rock at the laboratory scale

Shokouhi, P., Jin, J., Manogharan, P., Wood, C., Rivière, J., Elsworth, D. and Marone, C.
The Pennsylvania State University, University Park, PA, USA

ABSTRACT: We report on a series of laboratory experiments designed to simulate local effective stress field fluctuation and its influence on the evolution of permeability and dynamic stiffness in fractured samples of Westerly Granite. L-shaped samples are loaded with tri-axial stresses and fractured in situ. The fracture is subsequently sheared in two 4-mm steps. Oscillatory changes in the local effective stress field are imposed through application of normal stress or pore water pressure oscillations with varying amplitudes and frequencies. Active ultrasonic data (ultrasonic waves transmitted across the fracture) is used to monitor the evolution of wave velocity and attenuation before, during and after dynamic stressing. Throughout the experiment, the evolution of permeability is concurrently measured to determine the relationship between fracture permeability and nonlinear elastodynamic properties (stress-dependency of wave velocity and attenuation). Our results to date indicate that relative changes in wave velocity and permeability, due to both normal stress and pore pressure oscillations, are correlated, such that larger drops in wave velocity correspond to larger increases in permeability. Shearing of the fracture reduces the nonlinearity measured during normal stress oscillations for both rock samples. After shearing, the oscillations become generally less effective in enhancing the fracture permeability.

1. MOTIVATION AND BACKGROUND

In the context of induced seismicity due to fluid injection, of particular concern are dynamic stresses associated with injection, pumping and transport of supercritical H_2O–CO_2 fluids. These stresses may pose significant risk associated with accelerated deformation, fault reactivation and possible damage to reservoir seals. Regional increases in seismic activity induced by such dynamic stresses have been reported in numerous studies (Healy et al., 1968; Raleigh et al., 1976; Simpson et al., 1988; Davis and Pennington, 1989; Sminchak and Gupta, 2003; Deichmann and Giardini, 2009; Frohlich, 2012; Horton, 2012; Zoback and Gorelick, 2012; Zoback, 2012; Brodsky and Lajoie, 2013; Ellsworth, 2013; Holland, 2013; van der Elst et al., 2013; McNamara et al., 2015; McGarr et al., 2015; Walsh and Zoback, 2015; Weingarten et al., 2015). The recent seismic activity in Ridgecrest California (Ross et al., 2019) and its impact on the community around Los Angeles and local geothermal energy production are stark reminders of the impact earthquakes can have on energy. However, in the context of energy recovery, these dynamic stresses may be beneficial via enhancing permeability. Transient permeability changes caused by dynamic stresses associated with passing seismic waves have been reported at the field scale and also demonstrated in laboratory experiments (Elkhoury et al., 2006; Faoro et al., 2009; Elkhoury et al., 2011; Faoro et al., 2012; Candela et al., 2014, 2015; Carey et al., 2015; Frash et al., 2016; Im et al., 2018; Ishibashi et al., 2018; Zhang et al., 2018; Shi et al., 2018; Ye and Ghassemi, 2018; Shi et al., 2019). These studies show that fluid injection and dynamic stresses combine to produce significant changes in permeability, fault stability and poromechanical properties of rock. Such effects have significant implications for fossil fuel production and geothermal energy.

On the other hand, a number of studies have shown that earthquakes and the ensuing seismic waves cause transient changes in rock stiffness in the vicinity of faults (Li et al., 1998, 2006; Niu et al., 2008; Brenguier et al., 2008; Wu et al., 2009; Brenguier et al., 2014). Similar behavior has been recorded at laboratory scale (Shokouhi et al., 2017a). The parallels between the observed transient changes in permeability and stiffness due to dynamic stress perturbations suggest a physical link between the nonlinear stiffness and hydraulic characteristics of fractures (e.g., Witherspoon et al., 1980; Gale, 1982; Brown, 1987; Pyrak-Nolte et al., 1987; Durham & Bonner, 1995; Zimmerman & Bodvarsson, 1996; Berryman et al., 2002; Berkowitz, 2002; Guéguen & Schubnel, 2003; Hofmann et al., 2005; Batzle et al., 2006; Xu et al., 2006). Existing studies on coupling

between stiffness and poromechanical behavior of fractured samples focus primarily on quasi-static stress protocols (Mavko, 2013; Nara et al., 2011; Petrovitch et al., 2013; Pyrak-Nolte and Nolte, 2016). In this study, we carry out well-controlled laboratory experiments to simulate dynamic stressing and illuminate the coupling between permeability transients and nonlinear elastodynamic response. This ongoing effort addresses the critical need for improved understanding of how fluid injection and associated changes in stresses influence seismic and hydromechanical properties of rock.

This paper provides a brief description of the experimental approach and summarizes our main findings to date. A more in-depth discussion on some of the presented results can be found in Shokouhi et al. (2019).

2. EXPERIMENTAL SETUP

We conducted laboratory experiments designed to investigate the influence of dynamic effective stress oscillations on the evolution of permeability and elastodynamic stiffness of fractures in Granite subject to shearing. L-shaped samples sandwiched between steel forcing blocks (with embedded ultrasonic piezoelectric transducers) were jacketed and placed inside a pressure vessel, itself inserted into a biaxial load frame as shown in **Figure 1a**. The samples were first saturated with deionized, de-aired water before being loaded to a normal stress and confining pressures of 20 MPa and 15 MPa, respectively. Subsequently, the samples were fractured in situ by applying a shear load in servo displacement-control. The fracture plane was guided by starter notches at the top and bottom of the sample in order to create reproducible quasi-planar fractures. Displacements of the

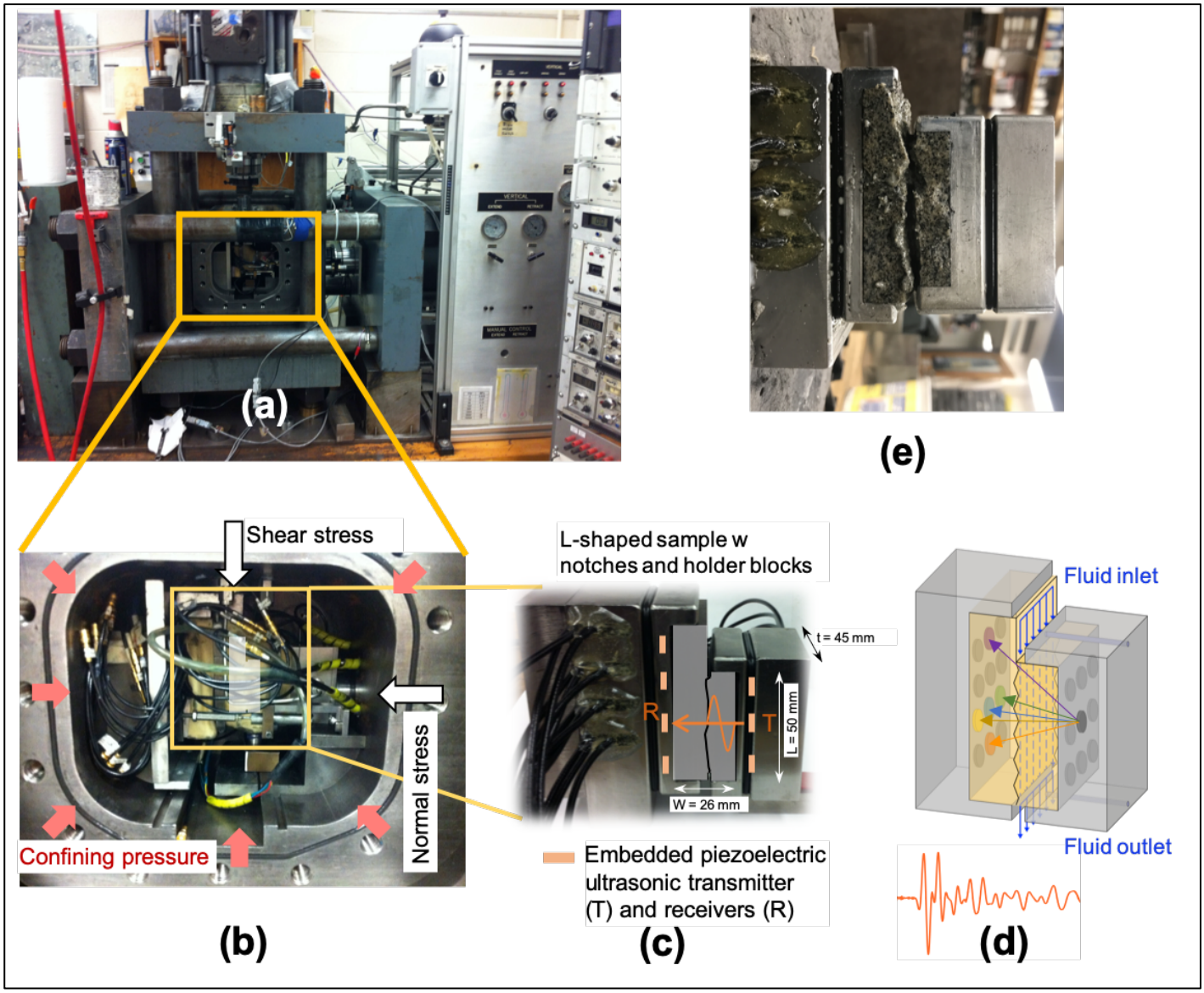

Figure 1 (a) The biaxial loading apparatus in Penn State's Rock Mechanics lab including (b) a pressure vessel to apply triaxial stress to the sample. (c) The L-shaped sample is sandwiched between two holder blocks with embedded piezoelectric transducers. (d) The experimental setup allows simultaneous measurements of flow and multi-channel ultrasonic data. (e) Picture of an in-situ fractured sample of Westerly Granite.

horizontal and vertical loading pistons were measured continuously using a pair of Direct Current Displacement Transducers (DCDTs). A Linear Variable Differential Transformer (LVDT) was placed inside the pressure vessel to allow for a redundant and more accurate measurement of displacement normal to the fracture plane. Deionized water was forced through the fracture via a differential pore pressure ($P_{p-inlet} = 4\ MPa$ and $P_{p-outlet} = 2\ MPa$) along the fracture length. The pore pressure intensifiers are independently servo-controlled and equipped with LVDTs to measure fluid flow rates into and out of the fracture plane (**Figure 1d**).

Changes in the applied effective stress field were imposed on the fractured samples were via pore pressure (P_p) and normal stress (σ_n) oscillations. Pore pressure oscillations were applied by oscillating $P_{p-inlet}$ while maintaining $P_{p-outlet}$ constant. Conversely, normal stress oscillations were applied by oscillating the horizontal piston of the load frame at prescribed amplitudes and frequencies. Multiple sets of dynamic stress oscillations of varying amplitude (~0.01 up to about ±1 MPa) and frequency (0.1, 1, 10 and 40 Hz) were applied to investigate the repeatability as well as amplitude and frequency dependencies of the measured response. A multi-channel data acquisition system was used to record ultrasonic data in both active and passive modes. Ultrasonic waves (with a center frequency of ~500 kHz) transmitted across the fracture (active mode) were used to monitor the evolution of wave velocity and amplitude before, during and after dynamic stressing. The active ultrasonic data are used to determine changes in elastodynamic properties and fracture stiffness due to the imposed oscillations. After applying a series of normal stress and pore water pressure oscillations, the fracture was sheared in two 4-mm steps (a total of 8mm). The dynamic stress oscillation protocol was executed repeatedly after each shearing step. During fracturing and shearing, the seismicity along the fracture was monitored passively in acoustic emission (AE) mode. Throughout the experiment, the evolution of flow rates at inlet and outlet was used to determine the stress-induced changes in permeability and ultimately to investigate the relationship between fracture permeability, aperture and stiffness. Finally, high-resolution optical profilometry was used to measure the roughness across the two post-mortem fractured surfaces in order to reconstruct fracture aperture distribution (results not shown in this paper).

Here, we summarize the main findings from the experiments on two Westerly granite samples WG1 (experiment p4966) and WG2 (experiment p4975) obtained using multiple ultrasonic transmitter-receiver pairs shown in **Figure 1d**. Reporting the results from multiple transmitter-receiver pairs sets this paper apart from our recently-published closely related publication (Shokouhi et al., 2019). Also in this paper, we compare the results before and after shearing the fracture.

3. NONLINEARITY OF THE ELASTODYNAMIC RESPONSE: TRANSIENT CHANGES IN STIFFNESS WITH DYNAMIC STRESSING AND SHEAR

We measure the nonlinearity of the elastodynamic response directly by quantifying the stress-dependency of wave velocity and amplitude. **Figure 2** depicts the typical response of our fractured samples to dynamic stress perturbations. Immediately after effective stress oscillations, the fractured rock exhibits an instantaneous softening i.e., the wave velocity c_0 suddenly drops. However, if the dynamic perturbation is not too strong, this softening is transient; once the oscillation is removed, the velocity slowly recovers toward the pre-oscillation wave velocity c_0. Note that during the oscillations, the wave velocity oscillates in response to dynamic stressing at frequencies that are harmonics of the excitation frequency. The average amplitude of these oscillations (at the oscillation frequency) is denoted as dc in **Figure 2**. If the stress oscillations persist, the changes in wave velocity reach a non-equilibrium steady state. This characteristic response (transient softening, slow recovery and velocity fluctuations) is a signature of nonlinear mesoscopic elasticity (Guyer and Johnson, 2009) and rich

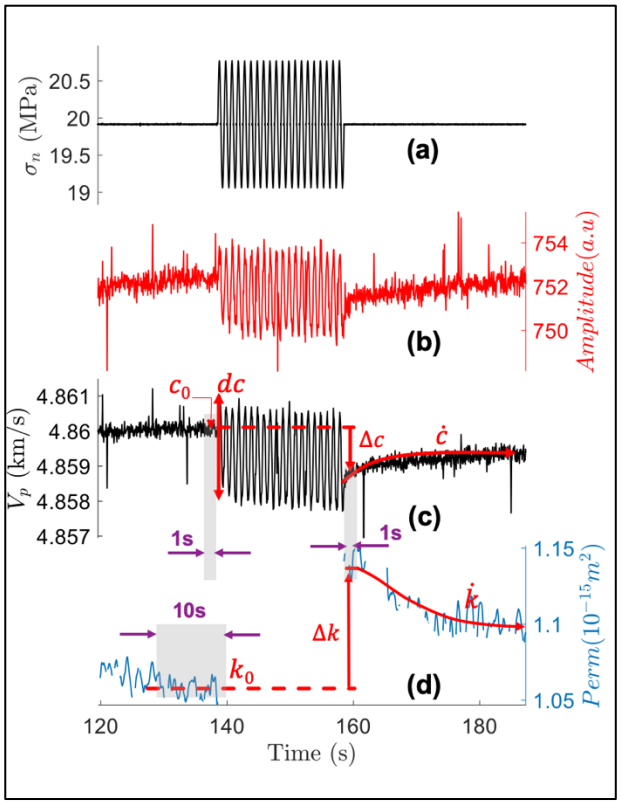

Figure 2. Typical response of fractured rock to stress perturbation: (a) imposed normal stress oscillations, the resulting evolutions of (b) ultrasonic wave amplitude, (c) velocity and (d) permeability with time.

in information on microstructure, fractures and contact mechanics. In comparison, the wave velocity in a linear elastic medium is stress-invariant i.e., $c = c_0$ before, during and after stress oscillations. Most intact rocks exhibit some degree of nonlinearity due to soft grain boundaries and microcracks in their matrix (Rivière et al., 2015). However, when fractured, their nonlinear electrodynamic responses are also influenced by the contact acoustic nonlinearity (CAN) at the rough fractured interface.

In order to quantify the nonlinearity of the fractures, we first obtain the evolution of ultrasonic wave amplitude (**Figure 2b)** and velocity (**Figure 2c)** from the continuously measured ultrasonic data (Shokouhi et al., 2019) and calculate three parameters: (1) the average or DC-change in wave velocity due to the imposed oscillations, (2) the amplitude of steady-state velocity fluctuation during the oscillations, and (3) the recovery rate of wave velocity post oscillation (**Figure 2c**). The relative velocity change ($\Delta c/c_0$) is defined as the % change in velocity due to the imposed normal stress or pore pressure oscillation. We calculate $\Delta c/c_0$ from the velocity before (c_0) and after (c) each oscillation averaged over 1-s time windows as depicted in **Figure 2c**. At a given oscillation amplitude, the more negative the $\Delta c/c_0$ (larger absolute value), the more nonlinear is the fracture. The parameter $\mathrm{d}c/c_0$ is defined as the amplitude of velocity oscillations, averaged over the oscillation duration and normalized by pre-oscillation velocity c_0 (**Figure 2c)**. Similar to $\Delta c/c_0$, a larger magnitude of $\mathrm{d}c/c_0$ at a given oscillation amplitude is an indication of higher nonlinearity. The third parameter $\dot{c}$ is defined as the (logarithmic) rate of recovery of wave velocity after the oscillation is removed (**Figure 2c)**. Materials of higher nonlinearity are expected to have slower recoveries (Shokouhi et al., 2017b).

In the next section, we discuss the dependence of $\Delta c/c_0$, $\mathrm{d}c/c_0$ and $\dot{c}$ (**Figure 3**) on the imposed normal stress and pore pressure amplitudes as well as frequency. In addition, we compare the measured nonlinearities before and after shearing the fracture. This comparison provides insight into how changes in the aperture size distribution (due to shearing and wear) and the presence of fines alter the fracture stiffness and the stress-dependency of the elastodynamic response. Although not shown here, similar nonlinearity parameters may be extracted from the evolution of ultrasonic wave amplitude (**Figure 2b**).

3.1. Oscillation Amplitude- and Frequency-Dependencies

The details on amplitude- and frequency-dependencies of $\Delta c/c_0$ and $\mathrm{d}c/c_0$ for a single transmitter-receiver pair are given in Shokouhi et al. (2019). Similar trends are observed for all transmitter-receiver pairs and therefore, not repeated here. In summary, the results given in Shokouhi et al. (2019) indicate that $\Delta c/c_0$ and $\mathrm{d}c/c_0$ are modulated by dynamic stress amplitudes for both pore pressure oscillations and fracture normal stress oscillations (**Figure 3** and **Figure 4**). In addition, the measurements exhibit frequency-dependence (not shown

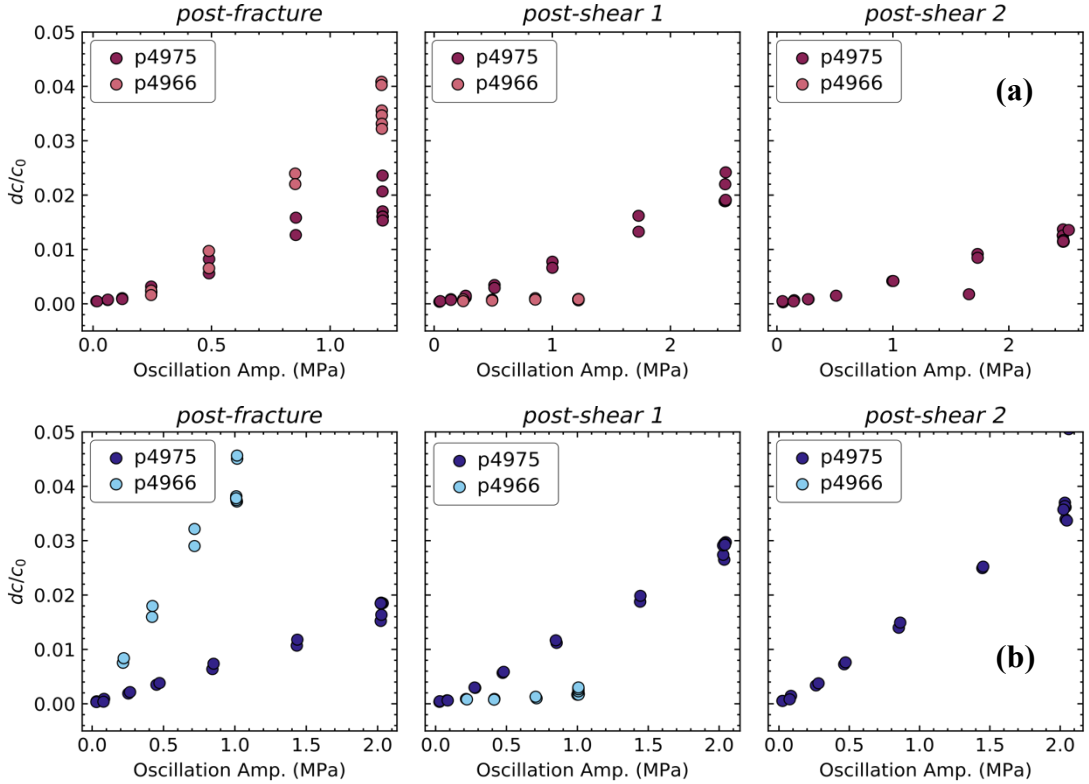

Figure 3 Amplitude-dependency of dc/c_0 post fracture (left panels), after shear step 1 (middle panels) and after shear step 2 (right panels) calculated for (a) normal stress and (b) pore pressure oscillations.

here); $\Delta c/c_0$ increases with the oscillation frequency, while $\mathrm{d}c/c_0$ mostly decreases. Observing different trends for the different nonlinearity parameters is not surprising. Although the origins of $\Delta c/c_0$ and $\mathrm{d}c/c_0$ remain unclear, there is empirical evidence that they stem from different micro-mechanical mechanisms (Rivière et al., 2016, 2015). Although the $\dot{c}$ values tend to generally increase with the oscillation amplitude, we do not observe a clear trend (not shown). This could be in part due to the variability in $\dot{c}$ caused by the low signal-to-noise ratio. The recovery rate $\dot{c}$ does not show a systematic dependency on frequency (not shown).

3.2. *Influence of Shearing*

Shearing of the fracture reduces $\mathrm{d}c/c_0$ during normal stress oscillations (**Figure 4a**). Interestingly, we have recorded different post-shear behavior for normal stress vs. pore pressure oscillations; the shearing increases the nonlinearity during pore pressure oscillations for one sample (p4975), while decreasing it for the other sample (p4966) (**Figure 4b**). This and other observations indicate possible differences in mechanisms activated during these two modes of dynamic stressing. On the other hand, shearing does not have a significant influence on $\Delta c/c_0$. The second shearing step decreases the measured nonlinearity $\Delta c/c_0$ but only slightly.

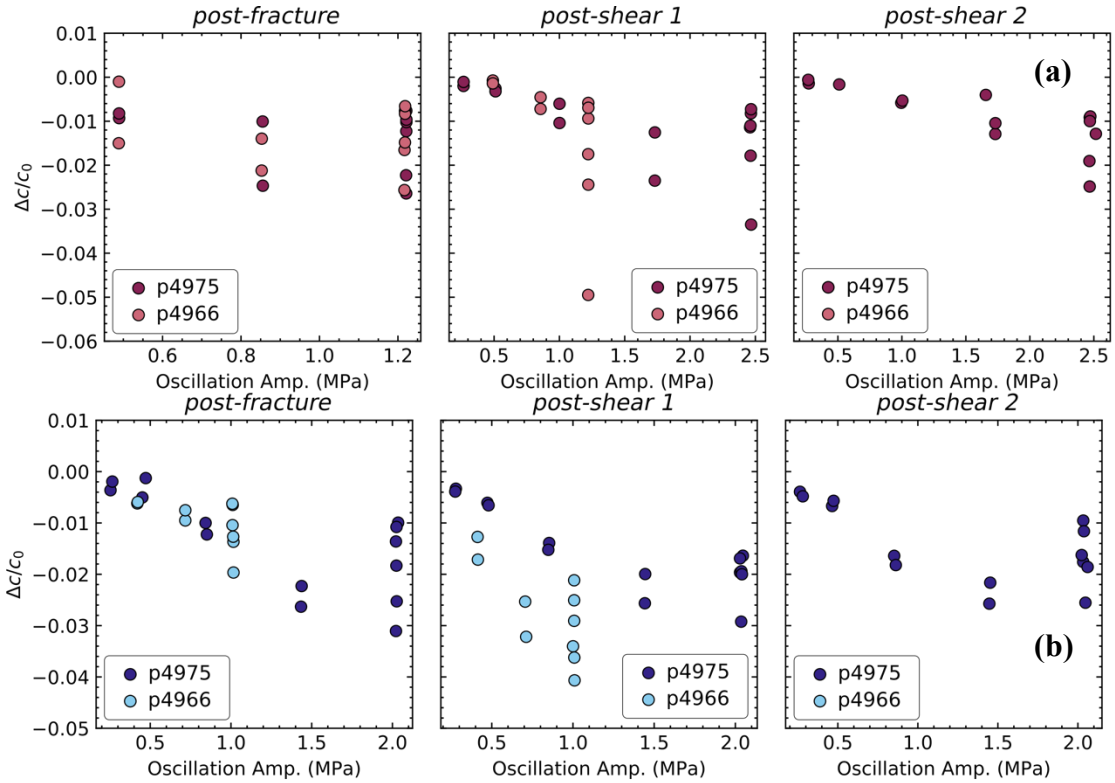

Figure 4 Amplitude-dependency of $\Delta c/c_0$ post fracture (left panels), after shear step 1 (middle panels) and after shear step 2 (right panels) calculated for (a) normal stress and (b) pore pressure oscillations.

4. PERMEABILITY EVOLUTION: TRANSIENT CHANGES WITH DYNAMIC STRESSING AND SHEAR

The stress-induced changes in permeability are captured by two parameters: (1) The transient change in permeability $\Delta k/k_0$ defined as the % change due to the imposed normal stress or pore pressure oscillations, normalized by the pre-oscillation permeability k_0 as illustrated in **Figure 2c** (Candela et al., 2014) and (2) The recovery rate of permeability after the transient increase $\dot{k}$.

4.1. *Oscillation Amplitude- and Frequency-Dependencies*

The dependencies of $\Delta k/k_0$ on the amplitude (**Figure 5**) and frequency of normal stress and pore pressure oscillations are given in Shokouhi et al. (2019). One important observation is that although small-amplitude oscillations (< 0.5MPa) may result in a decrease in permeability, large-amplitude oscillations generally increase permeability transiently. Furthermore, for the same oscillation amplitude and frequency, the pore pressure oscillations appear to be more effective in permeability enhancement ($\Delta k/k_0 > 0$) than the normal stress oscillations by a factor of ~2.5, particularly for sample WG1. In addition, $\Delta k/k_0$ increases, albeit slightly, with the frequency of oscillations (not shown here). The only exception is the decrease in $\Delta k/k_0$ for sample WG2, when we increase the fluid pressure oscillations from 1 Hz to 10 Hz. The details on amplitude- and frequency-dependencies of $\Delta k/k_0$ are given in Shokouhi et al. (2019). The recovery rate $\dot{k}$ does not show

clear amplitude- and frequency-dependencies (not shown here).

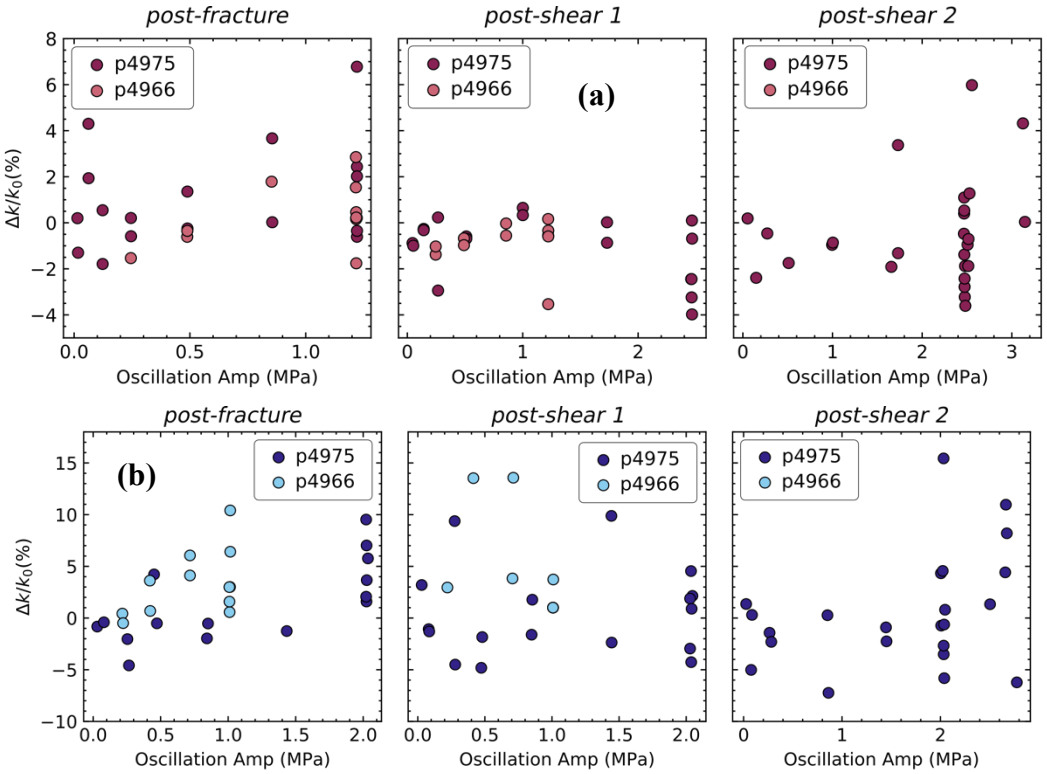

Figure 5. Amplitude-dependency of $\Delta k/k_0$ post fracture (left panels), after shear step 1 (middle panels) and after shear step 2 (right panels) calculated for (a) normal stress and (b) pore pressure oscillations.

4.2. Influence of Shearing

Generally speaking, after shearing the fracture, the normal stress oscillations become less effective in enhancing the fracture permeability (see **Figure 5a**). The trend is less obvious for pore water pressure oscillations (see **Figure 5b**).

5. CORRESPONDENCE BETWEEN STIFFNESS AND PERMEABILITY TRANSIENTS?

The main hypothesis driving this study was that the transient elastic softening is associated with a temporary increase in porosity and/or permeability, both of which are important for energy production and waste storage. Our results to date support this conjecture: the relative changes in wave velocity and permeability of fresh fractures (before shearing), due to both normal stress and pore pressure oscillations, are correlated, such that a larger drop in wave velocity (more negative $\Delta c/c_0$, equivalent to larger transient softening or higher nonlinearity) corresponds to a larger permeability enhancement $\Delta k/k_0$. As shown in **Figures 6a** and **6b (left panels)**, this overall correlation seems to hold for both normal stress and pore pressure oscillations. Furthermore, the recovery rates of wave velocity and permeability transients ($\dot{c}$ and $\dot{k}$) also seem to be correlated (**Figure 7**), although there is slightly more scatter. This observation further reinforces the presumed linkage between the evolution of fracture's elastodynamic and flow properties. In other words, the form of the measured permeability transients is similar to that for the nonlinear elastic effects and both recoveries follow the time-logarithmic trajectories observed in the field or in nature. We should note that the correlations shown in **Figure 6** correspond to $\Delta c/c_0$ averaged for 5 transducer pairs shown in **Figure 1d**. Examining the results for individual transducer pairs (not shown here) reveals the strong dependency of the measurements on the wave path. This is not surprising as the fracture aperture is nonuniform and the ray paths sample different portions of that interface.

Shearing the fracture appears to alter these relations indicating the influence of contact stiffness and shear fabric on both sets of properties (**Figure 6a** and **6b**). Overall, shearing seems to weaken the correlation between $\Delta c/c_0$ and $\Delta k/k_0$(**Figure 6a** and **6b, middle and right panels**). The question remains as to what underlying micro-mechanisms link the nonlinear elastodynamic behavior and hydraulic properties of fractures.

We considered two mechanisms for this observed correspondence: (1) the unclogging of fracture flow conduits via fluid pressure oscillations, and (2) the dependence of both properties on stress-induced changes in the fracture aperture. Previous work shows that particle clogging can alter permeability via dynamic stressing in

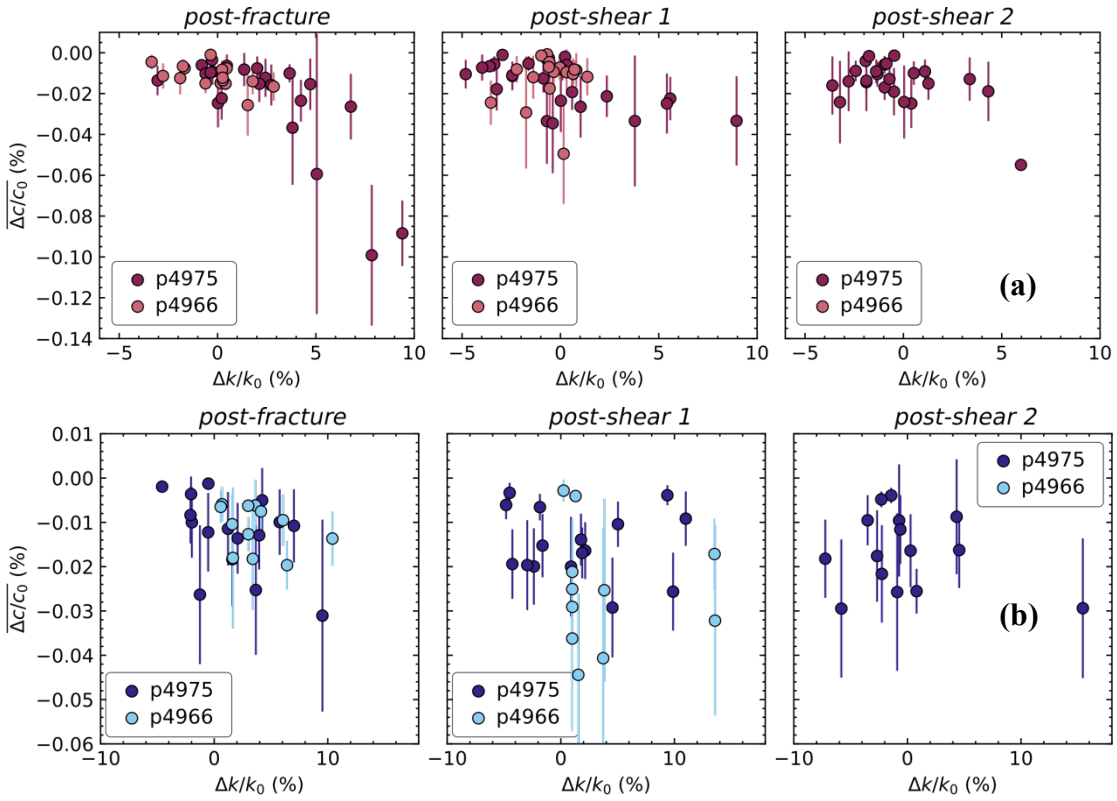

Figure 6. Correspondence between nonlinearity and permeability change due to (a) normal stress and (b) pore water pressure oscillations at three states: (left panel) post fracture, (middle panel) after shear step 1, and (right panel) after shear step 2. The nonlinearity is expressed in terms of average relative change in velocity due to imposed effective stress oscillations $\overline{\boldsymbol{\Delta c/c_0}}$. The $\overline{\boldsymbol{\Delta c/c_0}}$ values are averaged over the five wave paths depicted in Figure 1d.

Berea sandstone (Elkhoury et al., 2011; Candela et al., 2014, 2015). However, for fractures in Westerly Granite we observe an increase in permeability for both pore pressure and normal stress oscillations of sufficiently large amplitude. With the new insights from the coupled ultrasonic data, one may conclude that unclogging is merely one of many potential mechanisms.

The other explanation for the linkage between stiffness and flow properties of fractured rocks could be the dependence of both properties on the fracture aperture change due to the imposed stress oscillations. To further examine this hypothesis, we investigated whether $\Delta c/c_0$ or $\Delta k/k_0$ correlate with the measured changes in sample thickness changes (proxy for aperture compaction/dilation) during imposed oscillations (Shokouhi et al., 2019). However, we did not observe a strong correlation. This lack of strong correlation suggests that changes in fracture aperture cannot be the sole driving mechanism for permeability change, especially when driven by pore pressure oscillations.

We also used high-resolution optical profilometry to measure the roughness across the post-mortem fractured surfaces in order to reconstruct the fracture aperture distribution. However, since the fractures were created in-situ and were sheared twice before the roughness measurements, we do not have information on the aperture or roughness of fracture interfaces immediately post-fracture nor immediately post-shear (1st shearing step).

REFERENCES

Batzle, M.L., Han, D.-H., Hofmann, R., 2006. Fluid mobility and frequency-dependent seismic velocity — Direct measurements. Geophysics 71, N1–N9. https://doi.org/10.1190/1.2159053

Berkowitz, B., 2002. Characterizing flow and transport in fractured geological media: A review. Advances in Water Resources 25, 861–884. https://doi.org/10.1016/S0309-1708(02)00042-8

Berryman, J.G., Berge, P.A., Bonner, B.P., 2002. Estimating rock porosity and fluid saturation using only seismic velocities. Geophysics 67, 391–404. https://doi.org/10.1190/1.1468599

Brenguier, F., Campillo, M., Hadziioannou, C., Shapiro, N.M., Nadeau, R.M., Larose, E., 2008. Postseismic Relaxation Along the San Andreas Fault at Parkfield from Continuous Seismological Observations. Science 321,

1478–1481. https://doi.org/10.1126/science.1160943
Brenguier, F., Campillo, M., Takeda, T., Aoki, Y., Shapiro, N.M., Briand, X., Emoto, K., Miyake, H., 2014. Mapping pressurized volcanic fluids from induced crustal seismic velocity drops. Science 345, 80–82.
Brodsky, E.E., Lajoie, L.J., 2013. Anthropogenic Seismicity Rates and Operational Parameters at the Salton Sea Geothermal Field. Science 341, 543–546. https://doi.org/10.1126/science.1239213
Brown, S.R., 1987. Fluid flow through rock joints: The effect of surface roughness. Journal of Geophysical Research: Solid Earth 92, 1337–1347. https://doi.org/10.1029/JB092iB02p01337
Candela, T., Brodsky, E.E., Marone, C., Elsworth, D., 2015. Flow rate dictates permeability enhancement during fluid pressure oscillations in laboratory experiments: Dynamic permeability enhancement. Journal of Geophysical Research: Solid Earth 120, 2037–2055. https://doi.org/10.1002/2014JB011511
Candela, T., Brodsky, E.E., Marone, C., Elsworth, D., 2014. Laboratory evidence for particle mobilization as a mechanism for permeability enhancement via dynamic stressing. Earth and Planetary Science Letters 392, 279–291. https://doi.org/10.1016/j.epsl.2014.02.025
Carey, J.W., Lei, Z., Rougier, E., Mori, H., Viswanathan, H., 2015. Fracture-permeability behavior of shale. Journal of Unconventional Oil and Gas Resources 11, 27–43. https://doi.org/10.1016/j.juogr.2015.04.003
Davis, S.D., Pennington, W.D., 1989. Induced seismic deformation in the Cogdell oil field of west Texas. Bulletin of the Seismological Society of America 79, 1477–1495.
Deichmann, N., Giardini, D., 2009. Earthquakes Induced by the Stimulation of an Enhanced Geothermal System below Basel (Switzerland). Seismological Research Letters 80, 784–798. https://doi.org/10.1785/gssrl.80.5.784
Durham, W., Bonner, B., 1995. Closure and fluid flow in discrete fractures, in: Fractured and Jointed Rock Masses. Balkema Rotterdam, p. 446.
Elkhoury, J.E., Brodsky, E.E., Agnew, D.C., 2006. Seismic waves increase permeability. Nature 441, 1135–1138. https://doi.org/10.1038/nature04798
Elkhoury, J.E., Niemeijer, A., Brodsky, E.E., Marone, C., 2011. Laboratory observations of permeability enhancement by fluid pressure oscillation of in situ fractured rock. Journal of Geophysical Research 116. https://doi.org/10.1029/2010JB007759
Ellsworth, W.L., 2013. Injection-Induced Earthquakes. Science 341, 1225942. https://doi.org/10.1126/science.1225942
Faoro, I., Elsworth, D., Marone, C., 2012. Permeability evolution during dynamic stressing of dual permeability media. Journal of Geophysical Research: Solid Earth 117, n/a-n/a. https://doi.org/10.1029/2011JB008635
Faoro, I., Niemeijer, A., Marone, C., Elsworth, D., 2009. Influence of shear and deviatoric stress on the evolution of permeability in fractured rock. Journal of Geophysical Research: Solid Earth 114. https://doi.org/10.1029/2007JB005372
Frash, L.P., Carey, J.W., Lei, Z., Rougier, E., Ickes, T., Viswanathan, H.S., 2016. High-stress triaxial direct-shear fracturing of Utica shale and in situ X-ray microtomography with permeability measurement. Journal of Geophysical Research: Solid Earth 121, 5493–5508. https://doi.org/10.1002/2016JB012850
Frohlich, C., 2012. Two-year survey comparing earthquake activity and injection-well locations in the Barnett Shale, Texas. PNAS 109, 13934–13938. https://doi.org/10.1073/pnas.1207728109
Gale, J.E., 1982. The Effects Of Fracture Type (Induced Versus Natural) On The Stress-Fracture Closure-Fracture Permeability Relationships, in: ARMA-82-290. Presented at the The 23rd U.S Symposium on Rock Mechanics (USRMS), American Rock Mechanics Association, ARMA, p. 9.
Guéguen, Y., Schubnel, A., 2003. Elastic wave velocities and permeability of cracked rocks. Tectonophysics 370, 163–176. https://doi.org/10.1016/S0040-1951(03)00184-7
Guyer, R.A., Johnson, P.A., 2009. Nonlinear Mesoscopic Elasticity: The Complex

Behaviour of Rocks, Soil, Concrete. John Wiley & Sons.
Healy, J.H., Rubey, W.W., Griggs, D.T., Raleigh, C.B., 1968. The Denver Earthquakes. Science 161, 1301–1310.
Hofmann, R., Xu, X., Batzle, M., Prasad, M., Furre, A.-K., Pillitteri, A., 2005. Effective pressure or what is the effect of pressure? The Leading Edge 24, 1256–1260. https://doi.org/10.1190/1.2149644
Holland, A.A., 2013. Preliminary analysis of the 2013 Love County earthquake swarm. Oklahoma Geological Survey Open-File Report OF1 2013, 30.
Horton, S., 2012. Disposal of Hydrofracking Waste Fluid by Injection into Subsurface Aquifers Triggers Earthquake Swarm in Central Arkansas with Potential for Damaging Earthquake. Seismological Research Letters 83, 250–260. https://doi.org/10.1785/gssrl.83.2.250
Im, K., Elsworth, D., Fang, Y., 2018. The influence of Preslip Sealing on the Permeability Evolution of Fractures and Faults. Geophysical Research Letters 45, 166–175. https://doi.org/10.1002/2017GL076216
Ishibashi, T., Elsworth, D., Fang, Y., Riviere, J., Madara, B., Asanuma, H., Watanabe, N., Marone, C., 2018. Friction-Stability-Permeability Evolution of a Fracture in Granite. Water Resources Research 54, 9901–9918. https://doi.org/10.1029/2018WR022598
Li, Y.-G., Chen, P., Cochran, E.S., Vidale, J.E., Burdette, T., 2006. Seismic Evidence for Rock Damage and Healing on the San Andreas Fault Associated with the 2004 M 6.0 Parkfield Earthquake. Bulletin of the Seismological Society of America 96, S349–S363. https://doi.org/10.1785/0120050803
Li, Y.-G., Vidale, J.E., Aki, K., Xu, F., Burdette, T., 1998. Evidence of Shallow Fault Zone Strengthening After the 1992 M7.5 Landers, California, Earthquake. Science 279, 217–219. https://doi.org/10.1126/science.279.5348.217
Mavko, G., 2013. Relaxation shift in rocks containing viscoelastic pore fluids. GEOPHYSICS 78, M19–M28. https://doi.org/10.1190/geo2012-0272.1
McGarr, A., Bekins, B., Burkardt, N., Dewey, J., Earle, P., Ellsworth, W., Ge, S., Hickman, S., Holland, A., Majer, E., Rubinstein, J., Sheehan, A., 2015. Coping with earthquakes induced by fluid injection. Science 347, 830–831. https://doi.org/10.1126/science.aaa0494
McNamara, D.E., Hayes, G.P., Benz, H.M., Williams, R.A., McMahon, N.D., Aster, R.C., Holland, A., Sickbert, T., Herrmann, R., Briggs, R., Smoczyk, G., Bergman, E., Earle, P., 2015. Reactivated faulting near Cushing, Oklahoma: Increased potential for a triggered earthquake in an area of United States strategic infrastructure. Geophys. Res. Lett. 42, 2015GL064669. https://doi.org/10.1002/2015GL064669
Nara, Y., Meredith, P.G., Yoneda, T., Kaneko, K., 2011. Influence of macro-fractures and micro-fractures on permeability and elastic wave velocities in basalt at elevated pressure. Tectonophysics, Thermo-Hydro-Chemo-Mechanical Couplings in Rock Physics and Rock Mechanics 503, 52–59. https://doi.org/10.1016/j.tecto.2010.09.027
Niu, F., Silver, P.G., Daley, T.M., Cheng, X., Majer, E.L., 2008. Preseismic velocity changes observed from active source monitoring at the Parkfield SAFOD drill site. Nature 454, 204.
Petrovitch, C.L., Nolte, D.D., Pyrak-Nolte, L.J., 2013. Scaling of fluid flow versus fracture stiffness. Geophysical Research Letters 40, 2076–2080. https://doi.org/10.1002/grl.50479
Pyrak-Nolte, L.J., Myer, L.R., Cook, N.G.W., Witherspoon, P.A., 1987. Hydraulic and mechanical properties of natural fractures in low-permeability rock (No. LBL-22718; CONF-870815-2). Lawrence Berkeley Lab., CA (USA).
Pyrak-Nolte, L.J., Nolte, D.D., 2016. Approaching a universal scaling relationship between fracture stiffness and fluid flow. Nature Communications 7, 10663. https://doi.org/10.1038/ncomms10663
Raleigh, C.B., Healy, J.H., Bredehoeft, J.D., 1976. An Experiment in Earthquake Control at Rangely, Colorado. Science 191, 1230–1237.
Rivière, J., Pimienta, L., Scuderi, M., Candela, T., Shokouhi, P., Fortin, J., Schubnel, A.,

Marone, C., Johnson, P.A., 2016. Frequency, pressure, and strain dependence of nonlinear elasticity in Berea Sandstone. Geophysical Research Letters 43, 3226–3236. https://doi.org/10.1002/2016GL068061

Rivière, J., Shokouhi, P., Guyer, R.A., Johnson, P.A., 2015. A set of measures for the systematic classification of the nonlinear elastic behavior of disparate rocks. Journal of Geophysical Research: Solid Earth 120, 1587–1604. https://doi.org/10.1002/2014JB011718

Ross, Z.E., Idini, B., Jia, Z., Stephenson, O.L., Zhong, M., Wang, X., Zhan, Z., Simons, M., Fielding, E.J., Yun, S.-H., Hauksson, E., Moore, A.W., Liu, Z., Jung, J., 2019. Hierarchical interlocked orthogonal faulting in the 2019 Ridgecrest earthquake sequence. Science 366, 346–351. https://doi.org/10.1126/science.aaz0109

Shi, Y., Liao, X., Zhang, D., Liu, C., 2019. Seismic Waves Could Decrease the Permeability of the Shallow Crust. Geophysical Research Letters 46, 6371–6377. https://doi.org/10.1029/2019GL081974

Shi, Z., Zhang, S., Yan, R., Wang, G., 2018. Fault Zone Permeability Decrease Following Large Earthquakes in a Hydrothermal System. Geophysical Research Letters 45, 1387–1394. https://doi.org/10.1002/2017GL075821

Shokouhi, P., Rivière, J., Guyer, R.A., Johnson, P.A., 2017a. Slow dynamics of consolidated granular systems: Multi-scale relaxation. Appl. Phys. Lett. 111, 251604. https://doi.org/10.1063/1.5010043

Shokouhi, P., Rivière, J., Lake, C.R., Le Bas, P.-Y., Ulrich, T.J., 2017b. Dynamic acousto-elastic testing of concrete with a coda-wave probe: comparison with standard linear and nonlinear ultrasonic techniques. Ultrasonics 81, 59–65. https://doi.org/10.1016/j.ultras.2017.05.010

Simpson, D.W., Leith, W.S., Scholz, C.H., 1988. Two types of reservoir-induced seismicity. Bulletin of the Seismological Society of America 78, 2025–2040.

Sminchak, J., Gupta, N., 2003. Aspects of induced seismic activity and deep-well sequestration of carbon dioxide. Environmental Geosciences 10, 81–89. https://doi.org/10.1306/eg.04040302009

van der Elst, N.J., Savage, H.M., Keranen, K.M., Abers, G.A., 2013. Enhanced Remote Earthquake Triggering at Fluid-Injection Sites in the Midwestern United States. Science 341, 164–167. https://doi.org/10.1126/science.1238948

Walsh, F.R., Zoback, M.D., 2015. Oklahoma's recent earthquakes and saltwater disposal. Science Advances 1, e1500195. https://doi.org/10.1126/sciadv.1500195

Weingarten, M., Ge, S., Godt, J.W., Bekins, B.A., Rubinstein, J.L., 2015. High-rate injection is associated with the increase in US mid-continent seismicity. Science 348, 1336–1340.

Witherspoon, P.A., Wang, J.S.Y., Iwai, K., Gale, J.E., 1980. Validity of Cubic Law for fluid flow in a deformable rock fracture. Water Resources Research 16, 1016–1024. https://doi.org/10.1029/WR016i006p01016

Wu, C., Peng, Z., Ben-Zion, Y., 2009. Non-linearity and temporal changes of fault zone site response associated with strong ground motion. Geophysical Journal International 176, 265–278. https://doi.org/10.1111/j.1365-246X.2008.04005.x

Xu, X., Hofmann, R., Batzle, M., Tshering, T., 2006. Influence of pore pressure on velocity in low-porosity sandstone: Implications for time-lapse feasibility and pore-pressure study: Influence of pore pressure on velocity in sandstone. Geophysical Prospecting 54, 565–573. https://doi.org/10.1111/j.1365-2478.2006.00569.x

Ye, Z., Ghassemi, A., 2018. Injection-Induced Shear Slip and Permeability Enhancement in Granite Fractures. Journal of Geophysical Research: Solid Earth 123, 9009–9032. https://doi.org/10.1029/2018JB016045

Zhang, H., Wan, Z., Feng, Z., Wu, J., 2018. Shear-induced Permeability Evolution of Sandstone Fractures. Geofluids 1–11. https://doi.org/10.1155/2018/2416481

Zimmerman, R.W., Bodvarsson, G.S., 1996. Hydraulic conductivity of rock fractures. Transp Porous Med 23, 1–30. https://doi.org/10.1007/BF00145263

Zoback, M.D., 2012. Managing the seismic risk posed by wastewater disposal. Earth 57, 38.

Zoback, M.D., Gorelick, S.M., 2012. Earthquake triggering and large-scale geologic storage of carbon dioxide. Proceedings of the National Academy of Sciences 109, 10164–10168. https://doi.org/10.1073/pnas.1202473109